

Influence of hydrogen annealing on the properties of AZO thin films

IULIAN IORDACHE¹, ARCADIE SOBETKII², CĂTĂLIN VIȚELARU³, ELENA CHIȚANU^{1,*}, CRISTINA ANTONELA BANCIU^{1,*}, GABRIELA IOSIF¹, VIRGIL MARINESCU¹, GABRIELA SBÂRCEA¹, LEILA ACMOLA⁴, VALENTINA CĂPĂȚÎNĂ²

¹National Institute for Research and Development in Electrical Engineering ICPE-CA Bucharest, 313 Splaiul Unirii, 030138, Bucharest 3, Romania

²SC MGM STAR CONSTRUCT SRL, 7 Pâncota Street, 022773, Bucharest, Romania

³National Institute for Research and Development for Optoelectronics INOE 2000, 409 Atomiștilor Street, 077125, Măgurele, Romania

⁴„Alexandru Ioan Cuza” National Military College Constanța, 80 Dezrobirii Street, 900234, Constanța, Romania

The aim of this study was to obtain Al-doped ZnO (AZO) thin films by RF magnetron sputtering deposition with controllable structural, optical and electrical properties by adjusting the preparation process with a H₂ post-annealing treatment. The XRD pattern indicates the presence of single phase with hexagonal crystalline structure of ZnO. The AZO thin film obtained by 6 hours deposition process at a power density of ~7.5 W/cm² exhibited the best transparent conductive oxide (TCO) electrical and optical properties, reaching electrical resistivity of 2.74·10⁻³ Ω·cm, and an 80% transparency in the visible range.

(Received May 3, 2022; accepted June 7, 2022)

Keywords: AZO, Thin films, TCO, Magnetron sputtering

1. Introduction

Transparent conductive oxides (TCO) are widely used in a wide range of applications, from electronic devices that are currently used extensively in everyday life, to displays with special applications (nanomedicine), and to the classic solar cells [1]. In order to be used in new generation devices, the properties of TCO materials need to be improved by controllable methods. Doping ZnO with group III elements (aluminum [2], gallium [3] and indium [4]) results in controllable optical and electrical properties, in the sense of higher optical transmittance and better electrical conductivity (lower resistivity). Aluminum is the best candidate for doping ZnO due to its low price, non-toxicity and abundance. Studies carried out so far to obtain thin films of aluminum-doped ZnO have resulted in AZO films with good optical properties ($T > 80\%$), but in terms of electrical properties they have only reached resistivity in 10⁻³ Ω·cm domain. To improve the electrical conductivity, heat treatments were performed at different temperatures in a H₂ atmosphere [2].

In our study we developed a process for obtaining AZO thin films by RF magnetron sputtering method, followed by post-annealing treatment for controlling particles size, and corresponding structural, optical and electrical properties.

2. Experimental

2.1. AZO thin films depositions

AZO deposition target. Sintered ceramic target ZnO:Al₂O₃ (90:10 wt.%) with 2 inch diameter was prepared by a traditional ceramic process (1350°C), using ZnO and Al₂O₃ high purity powders (≥ 99.995%).

AZO thin films depositions. AZO thin films were deposited by RF magnetron sputtering method, using ZnO:Al₂O₃ (90:10 wt.%) target on SGG DIAMOND flat glass substrate with 4 mm thickness and 4 cm x 5 cm surface. Prior to use, the substrates were cleaned in Piranha bath followed by reactive ion etching with RF plasma for 5 min, ~10 W/cm², in argon (Ar), pressure 4x10⁻³ mbar using AJA model A320-XP system. The sputtering chamber was evacuated to less than 5x10⁻⁶ mbar before films depositions, performed in Ar gas with 5x10⁻³ mbar working pressure and ~7.5 W/cm² RF power for different deposition times 2 h, 4 h and 6 h respectively. After deposition AZO thin films were subjected to a treatment in H₂ atmosphere at 300°C for 1 hour.

The obtained thin films, by RF magnetron sputtering deposition for 2 hour (AZO2h), 4 hour (AZO4h) and 6 hour (AZO6h), were annealed in H₂ atmosphere. The heat treatment was carried out according to the diagram represented in the Fig. 1, with a heating rate of 10°C/min until it reaches 300°C, maintained at this temperature for 1 hour and finally cooling freely down to room temperature.

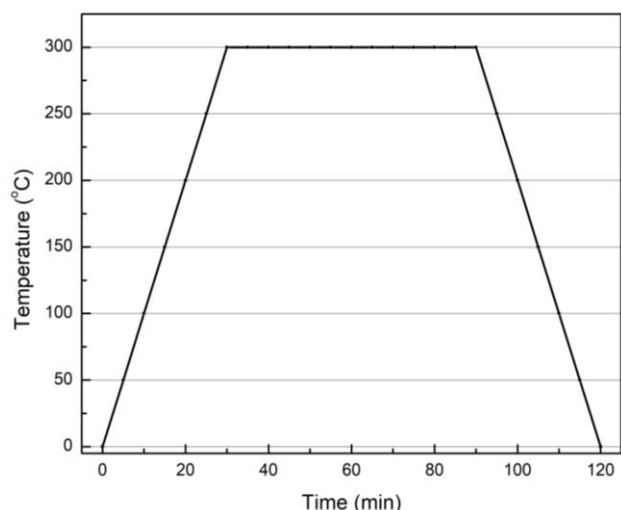


Fig. 1. Thermal treatment diagram for AZO thin films in H_2 atmosphere

2.2. Characterization

Film thickness was determined by surface profilometry with VEECO NT1100 system. Thin films were chemical acid etched to obtain a step profile that allows determining the film thickness. The 10X magnification lens and a 0.5X field of view (FOV) lens were used on $191 \mu\text{m} \times 255 \mu\text{m}$ surface.

Structural characterization of AZO thin films was achieved by X-ray diffraction in Bragg-Brentano θ - θ geometry, at room temperature with Bruker-AXS X-ray diffractometer type D8 Discover system. Analysis parameter X-ray tube with Cu anode, 40 kV/40 mA, 1D LynxEye detector, angular increment: 0.04° , angular measuring range $2\theta=10^\circ \div 100^\circ$.

Morphological characterization was performed with FESEM-FIB Scanning Electron Microscope (Workstation Auriga) equipped with a dispersive X-ray spectroscopy detector (Oxford Instruments). The images were recorded at 100kx magnification.

Optical characterization was realized with Jasco UV-VIS 570 Spectrophotometer, with double beam system (Czenry-Turner mount) that allows transmittance measurements in the UV/VIS/NIR range.

Electrical characterization was made using a Cascade C4S-64/50 with four-point probes placed at equal distances using a constant current source, Keithley 2400/2400-C SourceMeter; 200 V, 1 A, 20 W, for measuring electrical resistivity and surface resistance. Measurements were performed according to the method described in ASTM F 84-99 [5].

3. Results and discussion

AZO thin films for TCO applications must fulfill a number of criteria: uniform film with crystalline structure, controlled defects (by doping), high optical transparency and low electrical resistivity. These properties can be

achieved by several methods: doping with group III elements and/or by heat treatments in the reducing atmosphere (hydrogen). The annealing temperature in H_2 at 300°C was chosen because of several reasons. First of all, it is known that this is a temperature considered somehow the maximum allowed for the typical processing of an optoelectronic device on a glass support. In fact, we choose for a annealing treatment at the lowest possible temperature. It was also expected that this annealing temperature would not be high enough to cause a significant recrystallization of the films allowing us to investigate only the effect of hydrogen treatment [6, 7, 14]. Secondly, the H_2 annealed AZO thin films were obtained targeting optoelectronic applications where these depositions were made on the glass substrates type SGG Diamond extra float [8]. Higher annealing temperature than 300°C also may damage the glass substrate and the structures of designed devices. Thirdly, it is known that increasing time for H_2 annealing over 120 min. may lead to the increase in surface roughness which may cause deterioration of the electrical and optical properties [9, 10].

The obtained AZO thin films were analyzed by profilometry to determinate the average thickness of the deposited thin films. The film thickness increase with deposition time as follow $AZO_{2h} = 240\text{nm}$, $AZO_{4h} = 480\text{nm}$ and $AZO_{6h} = 720\text{nm}$.

All the samples were subjected to X-ray diffraction analysis. From XRD pattern recorded for all samples keep the same characteristic: 34° peak assigned to the (002) crystallographic plane (PDF 01-075-0576 ICDD [11]), with hexagonal structure and preferential orientation on the c-axis, perpendicular on substrate.

This is due to the change in crystal structure and is associated to film stress. No other peaks for Al_2O_3 or other related phases can be observed, which means that aluminum was incorporated in ZnO structure, by successfully replaced zinc in the hexagonal structure [12].

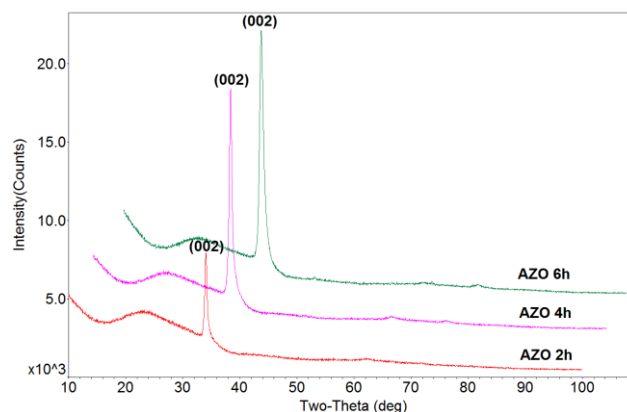


Fig. 2. The XRD pattern of AZO thin films (AZO_{2h} , AZO_{4h} and AZO_{6h}) (color online)

The crystallite size (D) are evaluated using Debye-Scherrer [13] mathematical model:

$$D = \frac{0.9}{\beta \cdot \cos \theta} \quad (1)$$

where λ is wavelength (1.5406 Å) of incident X-ray, β is the observed FWHM, and θ is the Bragg angle of diffraction peak. The crystallite size decrease from 19.5 nm for 2 hour deposition to 15.3 nm for 4 hour deposition and to a minimum of 11.9 nm for 6 hour deposition. This decrease, atypical for increasing deposition time, is due to post-annealed in H₂ [13]. During the magnetron sputtering process, bombardment with energetic oxygen ions takes place, which facilitates to obtain structures with a large number of oxygen-related defects (interstitial oxygen, oxygen at grain boundaries and oxygen vacancies). The annealing of AZO film in H₂ atmosphere at 300°C temperature, it can effectively remove defects based on oxygen, interstitial oxygen and oxygen at grain boundaries, as well as convert oxygen vacancies into HO groups [14]. As a result, these factors should be the main reasons for the decrease in particle size. Also, the removal of oxygen defects results in an increase in AZO film stress as well as dislocation density (Table 1).

Table 1. X-ray diffraction data

Sample	2θ (degree)	d (Å)	c (nm)	FWHM	Grain size (nm)	Dislocation density (x10 ¹⁶ lines/m ²)	Film Stress (x10 ⁻⁹ N/m ²)
AZO2h	34.038	2.6318	5.2456	0.426	19.5	0.26	-3.3
AZO4h	34.041	2.6315	5.2513	0.542	15.3	0.42	-3.8
AZO6h	34.041	2.6315	5.2631	0.699	11.9	0.70	-4.5

The amount of defects can be estimated by calculating dislocation density (δ) defined as length of dislocation lines per unit volume [15]:

$$\delta = \frac{1}{D^2} \text{ lines / m}^2 \quad (2)$$

Dislocations density (Table 1) for obtained films are slowly increases with film thickness from 0.26x10⁻¹⁶ lines/m² for AZO2h up to 0.70x10⁻¹⁶ lines/m² for AZO6h, confirming that the AZO films presents a crystal structure with small amount of defects (10⁻¹⁶ lines/m²) and with a good crystallinity.

From the XRD spectrum analysis it can be seen that the plane (002) peak shifts to lower angles than the standard data ($2\theta = 34.502^\circ$), which manifests itself by the elongation of the c-axis lattice constant. In the case of hexagonal structures with a preferential orientation on the c-axis, the film stress can be calculated based on the biaxial deformation model [16]:

$$\sigma = \left[2c_{13} - c_{33} (c_{11} - c_{12}) / c_{13} \right] \frac{c - c_0}{c_0} \quad (3)$$

where, c is the lattice constant for AZO film, c_0 is the corresponding bulk value (0.5206 nm), the values of elastic constants of single crystal ZnO used for c_{ij} are: $c_{11} = 2.1 \times 10^{11}$ N/m², $c_{33} = 2.1 \times 10^{11}$ N/m², $c_{12} = 1.2 \times 10^{11}$ N/m², $c_{13} = 1.05 \times 10^{11}$ N/m² [16]. Finally, the film stress can be expressed as:

$$\sigma = -4.5 \times 10^{11} \frac{c - c_0}{c_0} \quad (4)$$

From Table 1 can be seen the lattice constants for AZO films are changed comparative to bulk ZnO, which clearly suggests that the film grains are under stress due to changes in the concentration and nature of defects. These changes cause the elongation or compressions of lattice constants. In general internal stress of AZO films has the negative values, indicating compressive stress [17]. In general, thin film stress consists of two components: intrinsic stress due to the presence of impurities, characterized by defects and deformations in the crystal and extrinsic stress due to network thermal expansion and lattice mismatches between the film and the substrate. In the case of film with high thicknesses, the extrinsic stress is considerably diminished and the predominant is the intrinsic stress. From calculated values, it was observed that film intrinsic stress is increasing with film thickness, due to the decreasing of particle size and by the deformation of the crystal lattice.

The morphology of the surface was analyzed by scanning electron microscopy, the images obtained, Figs. 3-5, at 100kx magnifications, show that all samples consist of continuous and homogeneous films and present microcrystal regularly arranged on the substrate with a dimensional uniformity. Also, the increase of deposition time leads to elongated surface grains.

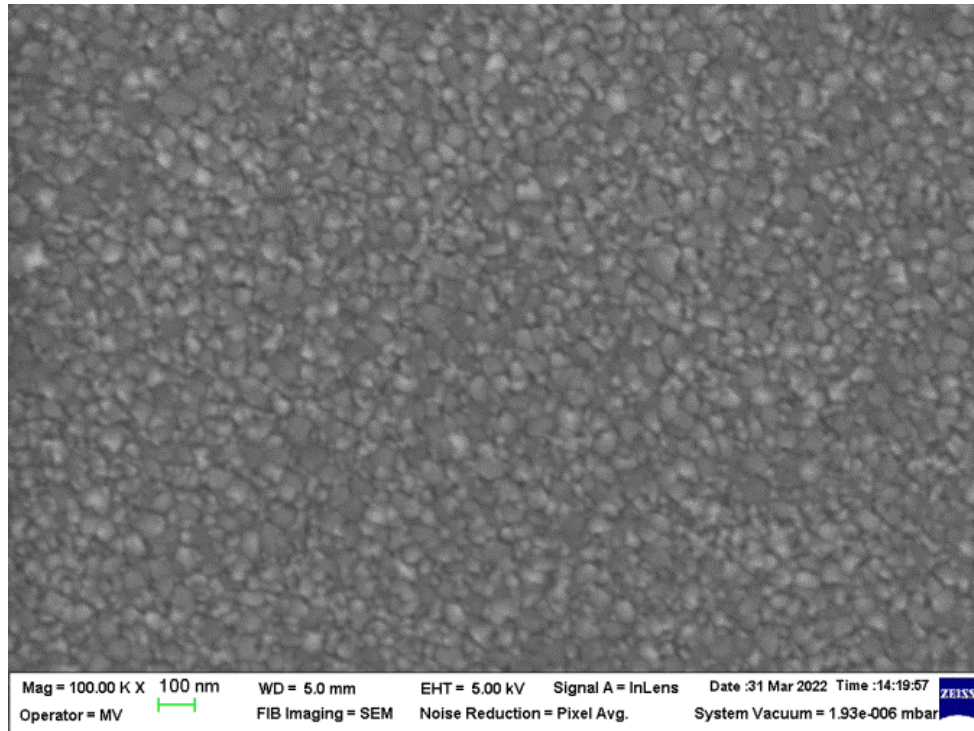


Fig. 3. SEM micrograph of AZO2h thin film (100kx)

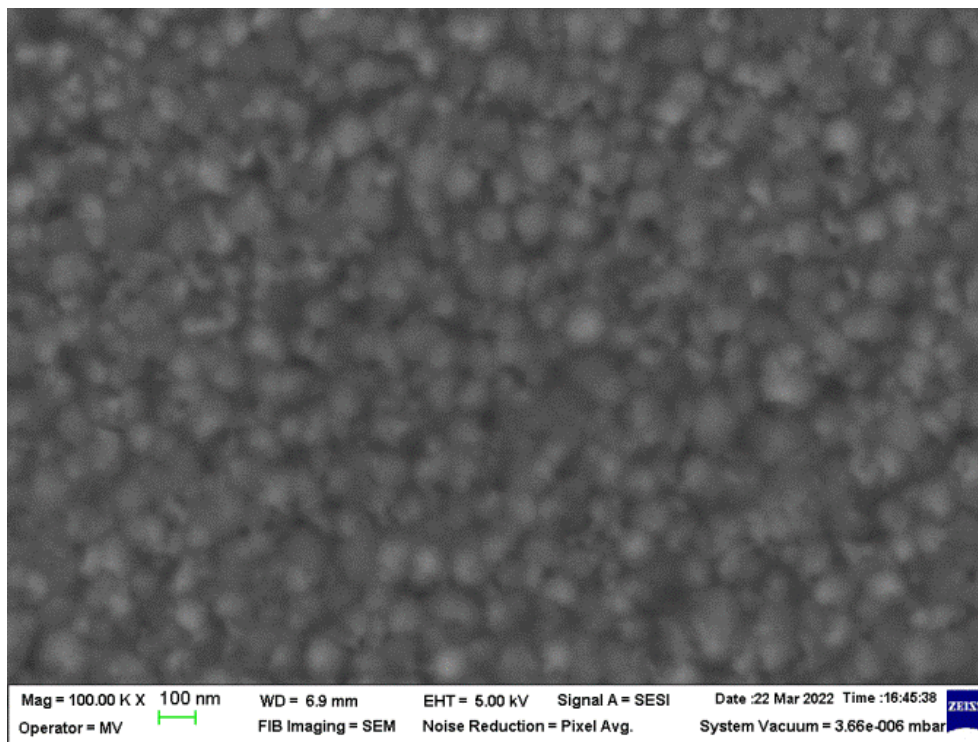


Fig. 4. SEM micrograph of AZO4h thin film (100kx)

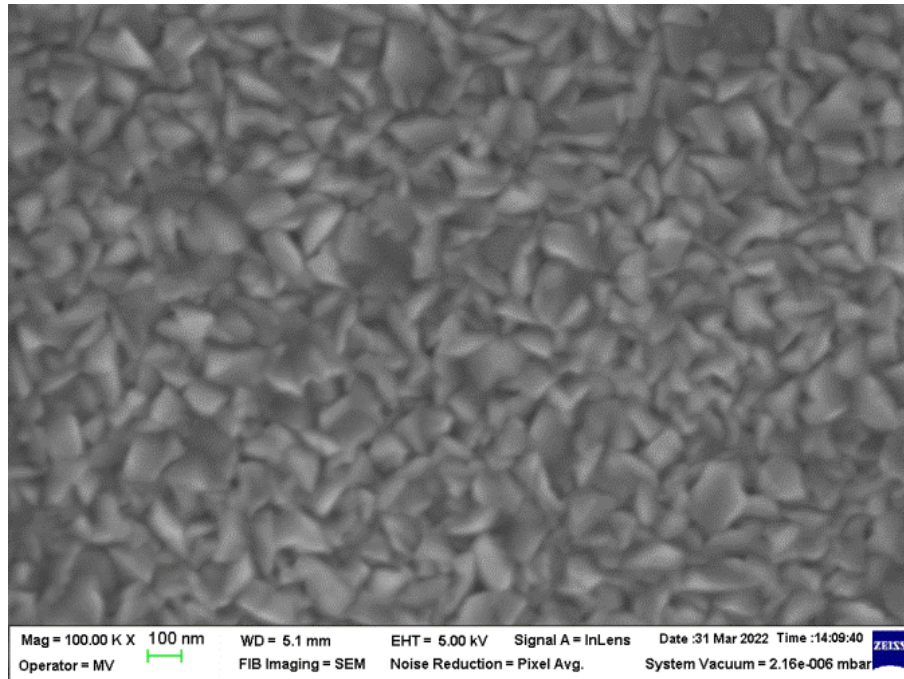


Fig. 5. SEM micrograph of AZO6h thin film (100kx)

Fig. 6 shows the variation of the optical transmission as a function of the wavelength for the UV-VIS domain (200-800 nm) for the SGG DIAMANT support glass and for AZO2h, AZO4h and AZO6h films. In the case of support glass, an exponential increase in UV range (200-400 nm) up to 90% can be observed, reaching an average value of 91.2% in the visible range.

AZO thin films show the same exponential increase in UV region, all samples reaching a maximum values about 84%. In the visible range (400-800 nm), interference fringes can be seen due to the different thicknesses of the samples, but at the same time the uniformity of the thin films is confirmed. The decrease in average optical transmission with the increasing of film thickness may be caused by the adsorption of free carriers, which in the case of thick films have a higher concentration [23], which leads to higher absorption.

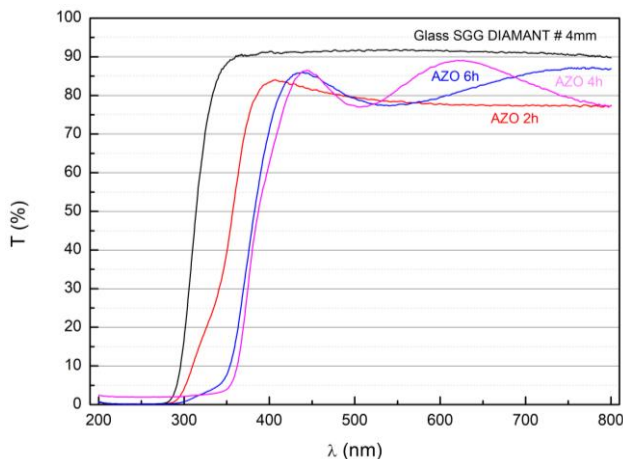


Fig. 6. The variation of transmittance with the wavelength in visible domain for AZO2h, AZO4h and AZO6h (color online)

The thin films deposited for duration of 2 hours have an average transmission value of 84%, AZO4h film an average optical transmission of 83% and the thickest film deposited 6 hours has an average transmission value of 80.2%. All analyzed samples show an average value of the optical transmission in the visible range higher than 80%, with good optical transparency.

The optical band gap, E_{go} , was calculated according to Tauc relationship [24]:

$$(\alpha h\nu)^{1/n} = A(h\nu - E_{go}) \quad (5)$$

where α is absorption coefficient, h is Planck's constant, ν is the frequency of incident photons and A is a constant. For materials with direct transition, in Tauc relations, $n = 1/2$ and for those with indirect transition $n = 2$ [20].

It has been found that the absorption coefficient of TCO films, such as AZO films, follows the relationship [21, 22]:

$$\alpha h\nu = A\sqrt{h\nu - E_{go}} \quad (6)$$

The AZO thin films are materials with direct transition, and the optical band gap is calculated using above Tauc equation.

The dependence $(\alpha h\nu)^2 \left[\frac{(eV)^2}{cm^2} \right]$, on the energy of the photons $(h\nu)[eV]$, shows that these materials are with direct band (direct transitions allowed). The optical band gap is obtained by extrapolating the linear portion of the absorption spectrum to $(\alpha h\nu)^2 = 0$. Graphs for TCO film show a linear portion that intercepts the energy axis at

certain values, E_{go} (eV), indicating a direct band material (direct permissible transitions).

To determine the optical bandgap, the linear portion from the graph $(\alpha hv)^2 = f(hv)$ was extrapolated to the x -axis of the $(\alpha hv)^2$ vs. hv plot and thus the optical band gap was obtained (Fig. 7).

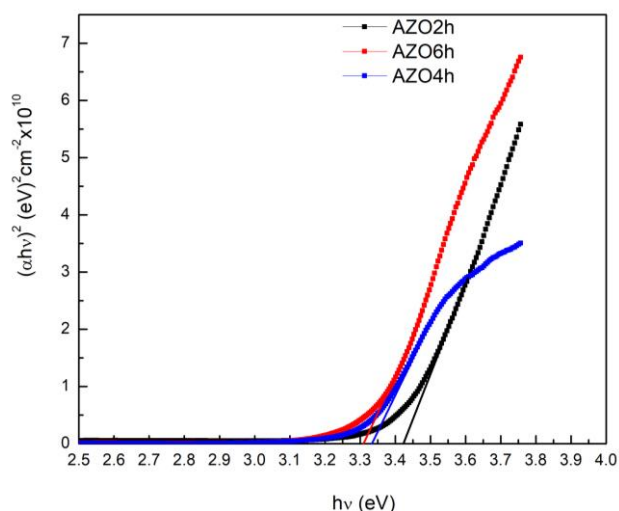


Fig. 7. Optical bandgap for AZO2h, AZO4h and AZO6h thin film (color online)

The band gap decreases from 3.43 eV for AZO2h, 3.34 eV for AZO4h and 3.31 eV for AZO6h (Table 2). The band gap energy of AZO films decreases with increasing thickness. In general, the variations of the band gap energy in ZnO-based thin films are related to changes in the average crystallite size and internal stress as well as electrical properties.

Table 2. Bandgap and resistivity of AZO thin films

Sample	ρ ($\times 10^{-3} \Omega \cdot \text{cm}$)	E_g (eV)
AZO2h	7.86	3.43
AZO4h	3.57	3.34
AZO6h	2.74	3.31

The electrical resistivity (Table 2) of the AZO thin films is influenced by the H₂ annealing treatment. Oxygen-based defects have a negative influence on electrical properties. Thus, interstitial oxygen traps free electrons and induces electric field distortions within the lattice [18], oxygen at grain boundaries can also trap free electrons in an electric field at the grain boundary, and oxygen vacancies behave as a neutral impurity. Another explanation may be related to annealing process at 300°C in H₂, this temperature is close to Zn melting point, which leads to bonds partial breaking in the material [18,19], facilitating the replacement of Zn²⁺ ions with Al³⁺ which results in a free electron and a structural change by reducing crystallite size [25] all this resulting in decreased resistivity.

Measurements have revealed that after H₂ annealed, resistivity decreases with 40-50% comparative with as-

deposited samples. Our measurements are consistent with the results obtained by a number of researchers in recent years [26, 27].

4. Conclusions

In this work, AZO thin films with structural, optical and electrical properties suitable for optoelectronic applications were successfully obtained. The AZO films obtaining process have RF magnetron sputtering deposition and H₂-annealing. The H₂-annealing process influences the crystallite structure, decreasing the particle size and leads to a lattice modification and implicitly to film stress. This behaviour is more pronounced for the film with the highest thickness. This decrease in crystallite size is due to the removal of oxygen-based defects introduced in the film during magnetron sputtering depositions. The reduction of these defects also leads to a decrease in film electrical resistivity.

In this study was developed a process for preparation of AZO thin films with controllable structural, optical and electrical properties by using H₂ post-annealing treatment.

Acknowledgments

This work has been funded by the financial support of UEFISCDI project no. 7PTE/2020, the Competitiveness Operational Programme, project no. 262/2020, My SMIS 122543, project no. P_40_403, My SMIS 105568, subsidiary ctr. 133 D3 MGM/2018, and the contract no. 25PFE/2021 (Romanian Ministry of Research, Innovation and Digitization).

References

- [1] R. A. Afre, N. Sharma, M. Sharon, M. Sharon, Rev. Adv. Mater. Sci. **53**, 79 (2018)
- [2] D. V. Hoang, N. H. Vu, N. T. Do, A. T. T. Pham, T. H. Nguyen, J.-L. Kuo, T. B. Phan, V. C. Tran, J. Materiomics **8**(1), 123 (2022).
- [3] A. Rayerfrancis, P. B. Bhargav, K. G. Kumar, N. Ahmed, C. Balaji, J. Optoelectron. Adv. M. **23**(5-6), 275 (2021).
- [4] K. Adaikalam, S. Valanarasu, A. M. Ali, M. A. Sayed, W. Yang, H.-S. Kim, J. Asian Ceram. Soc. **10**(1), 108 (2022).
- [5] ASTM F 84 – 99, Standard Test Method for Measuring Resistivity of Silicon Wafers With an In-Line Four-Point Probe (1999).
- [6] V. Gupta, A. Mansingh, J. Appl. Phys. **80**, 1063 (1996).
- [7] M. K. Puchert, P. Y. Timbrell, R. N. Lamb, J. Vac. Sci. Technol. A **14**, 2220 (1996).
- [8] Saint-Gobain Glass ROMANIA, Glass extra float clear, SGG DIAMANT 2015
- [9] S. Y. Myong, K. S. Lim, Appl. Phys. Lett. **82**, 3026 (2003).

- [10] K. Zhang, A. R. Forouhi, I. Bloomer, *J. Vac. Sci. Technol. A* **17**, 1843 (1999).
- [11] ICDD (2013) PDF-2 2013 (Database), International Centre for Diffraction Data, Newtown Square, PA, SUA, (2013).
- [12] A. Narjis, H. El Aakib, M. Boukendil, M. El Hasnaoui, L. Nkhaili, A. Aberkouks, A. Outzourhit, *J. King Saud Univ. Sci.* **32**, 1074 (2020).
- [13] S. Yin, M. M. Shirolkar, J. Li, M. Li, X. Song, X. Dong, H. Wang, *AIP Adv.* **6**, 065020 (2016).
- [14] B.-Y. Oh, M.-C. Jeong, D.-S. Kim, W. Lee, J.-M. Myoung, *J. Cryst. Growth* **281**(2-4), 475 (2005).
- [15] E. Chitanu, *J. Optoelectron. Adv. M.* **23**(5-6), 270 (2021).
- [16] J. G. Lu, Z. Z. Ye, Y. J. Zeng, L. P. Zhu, L. Wang, J. Yuan, B. H. Zhao, *J. Appl. Phys.* **100**, 073714 (2006).
- [17] F. A. Garces, N. Budini, R. D. Arce, J. A. Schmidt, *Procedia Mater. Sci.* **9**, 221 (2015).
- [18] N. Akim, S. S. Cetin, M. Cakmak, T. Memmedli, S. Ozcelik, *J. Matter. Sci: Matter Electron* **24**, 5091 (2013).
- [19] J. Tauc, R. Grigorovici, A. Vancu, *Phys. Status Solidi B* **15**(2), 627 (1966).
- [20] N. Srinatha, Y. S. No, V. B. Kamble, S. Chakravarty, N. Suriyamurthy, B. Angadi, A. M. Umarji, W. K. Choi, *RSC Adv.* **6**, 9779 (2016).
- [21] A. Ashour, H. H. Afifi, S. A. Mahmoud, *Thin Solid Films* **248**(2), 253 (1994).
- [22] F. Tepehan, N. Özer, *Sol. Energy Mater. Sol. Cells* **30**(4), 353 (1993).
- [23] A. Bikowski, K. Ellmer, *J. Appl. Phys.* **113**(5), 053710 (2013).
- [24] K. D. A. Kumer, S. Valanarasu, S. Rex Rosario, V. Ganesh, Mohd. Shkir, C. J. Sreelatha, S. AlFaify, *Solid State Sci.* **78**, 58 (2018).
- [25] K.D.A. Kumar, S. Valanarasu, A. Kathalingam, V. Ganesh, M. Shkir, and S. AlFaify, *Appl. Phys. A* **123**, 801 (2017).
- [26] Y. M. Lin, C. H. Chu, H. W. Wu, Jow-Lay Huang, *Proceedings of the International MultiConference of Engineers and Computer Scientists 2015 Vol II*, IMECS 2015, March 18 - 20, 2015, Hong Kong
- [27] Y. H. Jeong, H. Chen, H. J. Jin, C. B. Park, *J. KIEEME* **22**, 320 (2009).

*Corresponding authors: elena.chitanu@icpe-ca.ro
cristina.banciu@icpe-ca.ro